The influence of fluid flow phenomena on the laser beam welding process ☆

Achim Mahrle, Jürgen Schmidt *

Institute of Fluid Dynamics and Thermodynamics, Otto-von-Guericke University Magdeburg, P.O. Box 4120, D-39016 Magdeburg, Germany

Abstract

A mathematical model for the simulation of characteristic weld pool phenomena during deep penetration laser beam welding based on a numerical solution of the conservation equations of energy, momentum and mass is presented. The modelling is carried out in dimensionless form and the various melt pool effects are investigated separately with regard to dependence on characteristic dimensionless groups. The developed three-dimensional simulation model allows numerical experiments in order to investigate the influence of the fluid dynamics in the fusion zone on the local temperature distribution. To assess the accuracy of the predicted weld pool shapes and sizes, the computed and experimentally determined seam widths of laser beam welded joints are compared for welds on different steels. © 2002 Published by Elsevier Science Inc.

1. Introduction

The simulation and analysis of the physical behaviour of welds usually requires the computation of the transient temperature field during the welding process. For a given material and joint design, this temperature distribution determines the microstructure in the heat-affected zone as well as residual stresses and distortions of the welding construction (Radaj, 1992). Therefore, the temperature field is fundamental to understand and analyze heat effects of welding and weld defects.

Important for the accurate prediction of the transient temperature field is the modelling of the energy input from the localized intense welding heat source into the workpiece and a realistic description of the heat transfer in the fusion zone. This so-called process modelling which should answer questions regarding the geometry of the fusion zone, the stability of the welding process and the welding efficiency, is strongly dependent on the selected welding method (Radaj, 1999). Because the physical mechanisms involved are concentrated to a small area, the investigation of the steady-state relative to the moved welding heat source is often sufficient. Especially, in the case of welding on straight lines, constant welding power and constant welding travel speed, this assumption can be regarded as a good approximation.

In the case of laser beam welding, which is one of the most progressive joining processes today, the necessary melting of the base material is realised by the use of laser beams. The attainable high power densities warm up the material up to boiling point temperature and this leads to the formation of a vapour capillary through the material, the so-called keyhole. This vapour channel which will be surrounded by a region of liquid material is kept open by a combination of the pressure of the plasma that forms in the keyhole and the recoil pressure of the evaporating metal (Dowden et al., 1987). The laser is moved relative to the workpiece with the welding travel speed, and the keyhole advances through the material along the welding groove. Most of the molten material flows around the keyhole, solidifies behind it as a result of heat transfer in the solid zone and forms, in this way, the weld seam (Hügel, 1992).

In recent years some computerized simulation models were developed for the theoretical analysis of the penetration mode laser beam welding process (Beck, 1996; Sudnik et al., 1996; Sudnik et al., 1998; Kern et al., 1998). Special problems are the modelling of the vapour channel formation with regard to dependence on the

---

* Corresponding author. Tel.: +49-391-67-18575; fax: +49-391-67-12762.

E-mail address: juergen.schmidt@vst.uni-magdeburg.de (J. Schmidt).

Nomenclature

a_0 thermal diffusity, m^2/s

A negative temperature coefficient of surface tension, N/(m K)

$c_{p,0}$ specific heat capacity at reference temperature, J/(kg K)

c^* dimensionless heat capacity

c^*_{eff} effective dimensionless heat capacity

g gravitational acceleration, m/s^2

h plate thickness, m

h_m enthalpy of melting, J/kg

$\tilde{H}^0$ standard enthalpy of adsorption, J/mol

k_l constant related to the entropy of segregation

l_{ch} characteristic length, m

p pressure, Pa

P_L laser power, W

$P_{L,abs}$ absorbed laser power, W

R, φ, Z dimensionless cylindrical coordinates

R_{max} dimensionless radial extension of domain Ω

$\tilde{R}$ gas constant, J/(mol K)

T absolute temperature, K

U, V, W components of dimensionless velocity vector

w_{ch} characteristic velocity, m/s

w_{key} vertical velocity on the keyhole boundary, m/s

Z_{max} dimensionless plate thickness

Greeks

β volumetric coefficient of expansion, K^{-1}

γ surface tension, N/m

Γ boundaries of domain Ω

Γ_{bot} bottom side of workpiece

Γ_{inf} inflow boundary

Γ_{key} keyhole bondary

Γ_{out} outflow boundary

Γ_s surface excess of the solute species at saturation, mol/m^2

Γ_{sym} symmetry area

Γ_{top} top side of workpiece

η_L thermal efficiency of laser

ϑ temperature, °C

ϑ_0 reference temperature, °C

ϑ_u environmental temperature, °C

ϑ_v boiling point temperature, °C

Θ dimensionless temperature

Θ_{liq} dimensionless liquidus temperature

Θ_m dimensionless melting point temperature

Θ_{sol} dimensionless solidus temperature

λ_0 thermal conductivity at reference temperature, W/(m K)

λ^* dimensionless thermal conductivity

v_0 kinematic viscosity at reference temperature, m^2/s

Π dimensionless pressure

ϱ_0 density at reference temperature, kg/m^3

ϱ^* dimensionless density

Ω computation domain

Characteristic dimensionless groups

$Gr = (g\beta l_{ch}^3 (\vartheta_v - \vartheta_u))/v_0^2$ Grashof number

$Ma = (l_{ch}\partial\gamma/\partial\vartheta(\vartheta_v - \vartheta_u))/(\varrho_0 v_0 a_0)$ Marangoni number

$Pe = (w_{ch}l_{ch})/a_0$ Péclet number

$Ph = (h_m)/(c_{p,0}(\vartheta_v - \vartheta_u))$ phase change number

$Pr = v_0/a_0$ Prandtl number

$Re = w_{ch}l_{ch}/v_0$ Reynolds number

$W_{key} = w_{key}/w_{ch}$ dimensionless velocity on the keyhole boundary

$Z_{max} = h/l_{ch}$ dimensionless ratio of plate thickness to keyhole radius

complex interactions between laser beam and material (Kroos et al., 1992; Beck et al., 1992; Kroos, 1993), and the correct prediction of the heat transfer in the fusion zone (Berger, 1993; Dowden et al., 1995; Becker, 1995; Matsunawa et al., 1998; Hügel et al., 1994). Especially, the fluid dynamics of the molten material influences the local temperature distribution and consequently the weld pool shape and size to a high degree. Its importance results from the high welding travel speeds and the complex flow conditions inside the weld pool. The latter are determined by the flow around the keyhole, surface tension, buoyancy forces as well as friction forces of the metal vapour escaping from the capillary (see Fig. 1). In order to enable a systematic investigation of these phenomena, a three-dimensional simulation program was developed (Mahrle and Schmidt, 2000, 2001). Compared
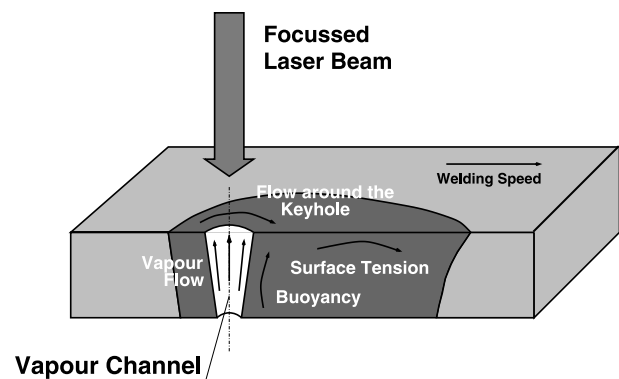
Fig. 1. Schematic illustration of deep penetration laser beam welding process and relevant phenomena in the fusion zone.

with other process models a strict dimensionless form has been used. This methodology minimizes the number of model parameters and enables the separate investigation of the above-mentioned melt pool effects with regard to dependence on the corresponding characteristic dimensionless group.

2. Modelling and numerical solution

In view of the present developments in research, the simulation of the local temperature distribution during deep penetration laser beam welding requires a three-dimensional modelling. Useful for the analysis of the fluid dynamics in the fusion zone is the assumption of the steady-state with a fully developed vapour channel, and without consideration of the complex physical mechanisms concerning the formation and stability of the keyhole and its interactions with the melt. In accordance to the main objective of the presented work, which is the description of the convective heat transfer in the molten zone and its influence on the weld pool shape and size, this approximation enables to reduce the modelling to the heat transfer in the liquid and solid phases. Furthermore, in the case of joining by welding of thin steel sheets, the radius of the vapour channel is assumed to be constant. So, the radius of the keyhole can be used appropriately as the characteristic length for the transformation of the governing equations into a dimensionless form. This methodology enables the simulation of the local temperature and velocity fields in the melt pool area as function of various dimensionless groups without knowledge of the accurate shape and size of the keyhole. However, proper values of this parameter can be derived by comparison of experimental measured and simulated temperature distributions.

For simplicity, the weld pool surface is regarded to be flat, and with this assumption, the choice of polar coordinates (R, φ, Z) is suitable. The origin of the coordinate system coincides with the centre line of the laser beam and the vapour channel, respectively (see Fig. 2). The computation domain Ω consisting of the weld pool and its surrounding area is described by

$$\Omega := \{ P = (R, \varphi, Z) \in \Re^3 :$$
$$1 \leqslant R \leqslant R_{\max}; \ 0 \leqslant \varphi \leqslant \pi; \ 0 \leqslant Z \leqslant Z_{\max} \} \qquad (1)$$

with the surface $\partial\Omega$ according to $\partial\Omega = \Gamma_{\text{key}} \cup \Gamma_{\text{inf}} \cup \Gamma_{\text{out}} \cup \Gamma_{\text{sym}} \cup \Gamma_{\text{top}} \cup \Gamma_{\text{bot}}$. $R_{\max}$ is the dimensionless radial extension of the domain Ω and $Z_{\max}$ is the dimensionless plate thickness and the ratio of real plate thickness to keyhole radius, respectively. Γ_{key} denotes the keyhole boundary, and Γ_{inf} and Γ_{out} are the inflow and the outflow boundaries. Γ_{sym} denotes the symmetry line, and Γ_{top} and Γ_{bot} are the top and the bottom side of the workpiece. Temperature and velocity field are coupled
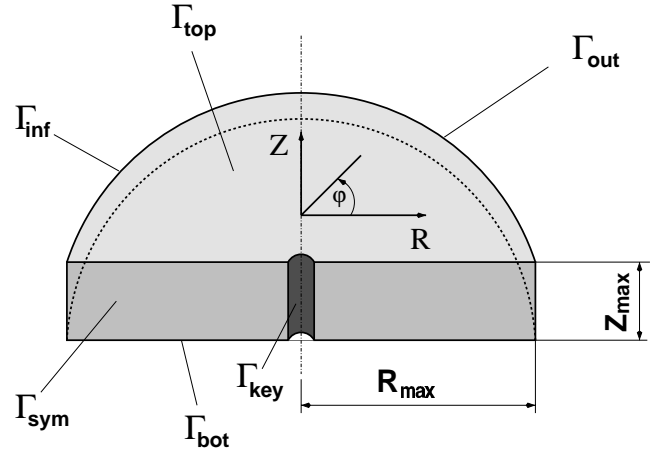
Fig. 2. Domain Ω for the computation of the local temperature field during deep penetration laser beam welding.

over the position of the melting point isotherm. Outside the weld pool area, the velocity corresponds to the welding travel speed. In the fusion zone, the solution of the conservation equations of energy, momentum and mass is necessary for the computation of the temperature and velocity distribution. Using cylindrical coordinates these equations can be written for the steady-state in the following dimensionless form:

$$\varrho^* c^* Pe \left[\frac{\partial(UR\Theta)}{\partial R} + \frac{\partial(V\Theta)}{\partial \varphi} + \frac{R\partial(W\Theta)}{\partial Z} \right]$$
$$= \frac{\partial}{\partial R}\left[R\lambda^* \frac{\partial\Theta}{\partial R} \right] + \frac{1}{R}\frac{\partial}{\partial \varphi}\left[\lambda^* \frac{\partial\Theta}{\partial \varphi} \right] + \frac{R\partial}{\partial Z}\left[\lambda^* \frac{\partial\Theta}{\partial Z} \right], \qquad (2)$$

$$Re\left[\frac{\partial(URU)}{\partial R} + \frac{\partial(VU)}{\partial \varphi} - V^2 + \frac{R\partial(WU)}{\partial Z} + \frac{R\partial\Pi}{\partial R} \right]$$
$$= \frac{\partial}{\partial R}\left[R\frac{\partial U}{\partial R} \right] - \frac{U}{R} + \frac{1}{R}\frac{\partial}{\partial \varphi}\left[\frac{\partial U}{\partial \varphi} \right] - \frac{2}{R}\frac{\partial V}{\partial \varphi} + \frac{R\partial}{\partial Z}\left[\frac{\partial U}{\partial Z} \right], \qquad (3)$$

$$Re\left[\frac{\partial(URV)}{\partial R} + \frac{\partial(VV)}{\partial \varphi} + UV + \frac{R\partial(WV)}{\partial Z} + \frac{\partial\Pi}{\partial \varphi} \right]$$
$$= \frac{\partial}{\partial R}\left[R\frac{\partial V}{\partial R} \right] - \frac{V}{R} + \frac{1}{R}\frac{\partial}{\partial \varphi}\left[\frac{\partial V}{\partial \varphi} \right] + \frac{2}{R}\frac{\partial U}{\partial \varphi} + \frac{R\partial}{\partial Z}\left[\frac{\partial V}{\partial Z} \right], \qquad (4)$$

$$Re\left[\frac{\partial(URW)}{\partial R} + \frac{\partial(VW)}{\partial \varphi} + \frac{R\partial(WW)}{\partial Z} + \frac{R\partial\Pi}{\partial Z} \right]$$
$$= \frac{\partial}{\partial R}\left[R\frac{\partial W}{\partial R} \right] + \frac{1}{R}\frac{\partial}{\partial \varphi}\left[\frac{\partial W}{\partial \varphi} \right] + \frac{R\partial}{\partial Z}\left[\frac{\partial W}{\partial Z} \right] + \frac{RGr\Theta}{Re}, \qquad (5)$$

$$\frac{\partial(RU)}{\partial R} + \frac{\partial V}{\partial \varphi} + \frac{R\partial W}{\partial Z} = 0 \qquad (6)$$

with the characteristic dimensionless groups Péclet number Pe, Reynolds number Re and Grashof number Gr. Péclet number and Reynolds number are coupled with the Prandtl number according to $Re = Pe/Pr$. The dimensionless temperature Θ is defined as $\Theta = (\vartheta - \vartheta_u)/(\vartheta_v - \vartheta_u)$, with the boiling point temperature ϑ_v and the temperature ϑ_u of the surroundings and the pre-heating temperature, respectively. The dimensionless pressure Π is given according to $\Pi = p/\varrho_0 w_{ch}^2$. U, V and W denote the components of the velocity vector which are normalised using the welding travel speed w_{ch}. The boundary conditions are specified as follows:

$$\partial V/\partial R = \partial W/\partial R = U = 0 \cup \Theta = 1 \quad \forall P \in \Gamma_{key}, \quad (7)$$

$$\partial U/\partial \varphi = \partial W/\partial \varphi = V = 0 \cup \partial \Theta/\partial \varphi = 0 \quad \forall P \in \Gamma_{sym}, \quad (8)$$

$$W = 0 \cup \partial \Theta/\partial Z = 0 \quad \forall P \in \Gamma_{top} \cup \Gamma_{bot}, \quad (9)$$

$$\partial U/\partial Z = -Ma/Pe \cdot \partial \Theta/\partial R \quad \forall P \in \Gamma_{top} \cup \Gamma_{bot}, \quad (10)$$

$$\partial V/\partial Z = -Ma/Pe \cdot \partial \Theta/R\partial \varphi \quad \forall P \in \Gamma_{top} \cup \Gamma_{bot}, \quad (11)$$

$$U = \cos(\varphi) \cup V = -\sin(\varphi) \cup W = 0 \cup \Theta = 0$$
$$\forall P \in \Gamma_{inf}, \quad (12)$$

$$U = \cos(\varphi) \cup V = -\sin(\varphi) \cup W = 0 \cup \partial \Theta/\partial R = 0$$
$$\forall P \in \Gamma_{out}. \quad (13)$$

The movement of the workpiece relative to the laser beam is considered in such a way that the constant welding travel speed is allocated to the computation domain outside the weld pool area. On the keyhole boundary a slip condition is assumed. The temperature is given as boiling point temperature, and so, the absorbed laser power is determined by the heat transfer into the liquid phase. Heat losses during the process are neglected. The temperature dependence of the material properties density ϱ^*, specific heat capacity c^* and heat conductivity λ^* is only considered in the solid state. For the fusion zone constant average values chosen as reference for the dimensionless form were used. The influence of the enthalpy of melting h_m is considered by increasing the specific heat capacity between solidus Θ_{sol} and liquidus temperature Θ_{liq} by the following formulation:

$$c_{eff}^* = c^* + \frac{h_m}{c_0(\vartheta_v - \vartheta_u)(\Theta_{liq} - \Theta_{sol})}$$
$$= c^* + \frac{Ph}{\Theta_{liq} - \Theta_{sol}} \quad (14)$$

A special problem is the specification of the Marangoni number Ma which characterises the influence of surface tension gradients. The temperature coefficient of surface tension $\partial \gamma/\partial \vartheta$ is only constant for pure metals. In alloys containing surface active solutes, this coefficient depends on temperature ϑ and activity a_i of the surface active species. For binary systems consisting of a metal and an alloying element, this dependence can be expressed by the formulation of Sahoo et al. (1988). It reads

$$\frac{\partial \gamma}{\partial \vartheta} = -A - \tilde{R}\Gamma_S \ln(1 + Ka_i) - \frac{Ka_i}{1 + Ka_i} \frac{\Gamma_S \Delta\tilde{H}^0}{T} \quad (15)$$

with A as the negative of the temperature coefficient of surface tension of the pure metal. $\tilde{R}$ denotes the gas constant, T the absolute temperature, Γ_S the surface excess of the solute species at saturation and $\Delta\tilde{H}^0$ the standard enthalpy of adsorption. The equilibrium constant K can be obtained via $K = k_l \exp(-\Delta\tilde{H}^0/\tilde{R}T)$, where k_l is a constant which is related to the entropy of segregation. For simplicity, only sulphur is considered as a surface active element which does not represent the total influence of all surface active elements. However, it can be regarded as sufficient for indicating the role of surface active elements and the determination of tendencies in the development of the weld pool shape and the temperature distribution in the heat-affected zone (Winkler et al., 1998). In Fig. 3 a plot of the temperature coefficient of surface tension of the Fe–S system versus temperature for different activities of sulphur is shown.

The solution of the governing differential Eqs. (2)–(6) with consideration of the boundary conditions (7)–(13) is carried out numerically by means of a finite difference method with a nonuniform gridspacing. In Fig. 4 the mesh near the keyhole area is shown. For the computation of the velocity distribution, the SMAC method on staggered grids (Naue and Bärwolff, 1992) was modified for the steady-state formulation. The resulting difference equation system is iteratively solved using the SOR method. For the verification of the implemented solution method different test cases were examined and the grid independence of the presented numerical results is ensured (Mahrle, 2000).
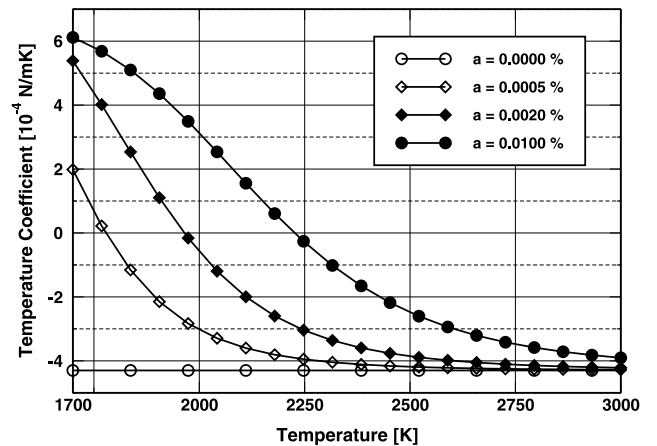
Fig. 3. Variation of the temperature coefficient of surface tension of Fe–S systems as a function of temperature and composition.
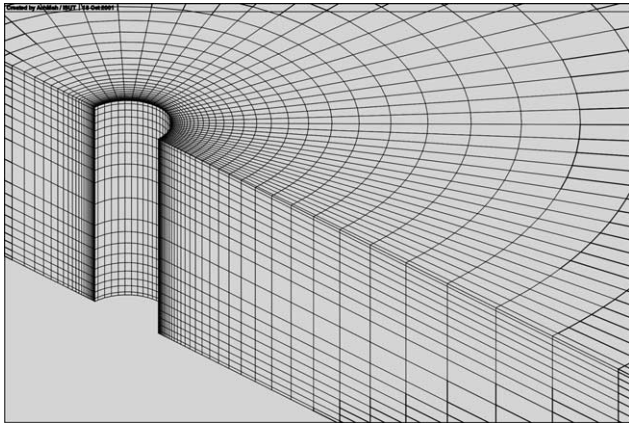
Fig. 4. Used mesh for the numerical solution near the keyhole boundary.

3. Results

For a given material with known density ϱ^*, specific heat capacity c^*, heat conductivity λ^*, melting point temperature Θ_m and phase change number Ph, the dimensionless temperature distribution $\Theta(R, \varphi, Z)$ is a function of the characteristic dimensionless groups Pe, Pr, Gr, Ma, W_{key} and Z_{max}. In fact, the Prandtl number as ratio of kinematic viscosity v_0 and thermal diffusivity a_0 is a material property too, but the knowledge of these

properties is insufficient for liquid metals, and in this context, the Prandtl number is used as model parameter.

In order to enable a separate investigation of the different melt pool effects, it is useful to vary only one parameter whereas the other dimensionless groups are assumed to be constant. As a first approach, the influence of surface tension gradients, buoyancy and friction forces were neglected. This leads to $Ma = Gr = W_{key} = 0$. The dimensionless temperature distribution is two-dimensional in this case and depends mainly on the Péclet number (Mahrle and Schmidt, 1998a,b). Fig. 5 shows calculated temperature and velocity fields for $Pe = 1$ and $Pe = 4$. The assumed values of the melting point temperature $\Theta_m = 0.5$ and the Prandtl number $Pr = 0.1$ are approximately valid for iron and steels, respectively.

For $Pe = 1$, the influence of the melt pool flow on the local temperature distribution and the resultant weld pool dimensions is negligible. However, as the Péclet number increases, two eddies are formed for $Pe = 4$. In contrast to the flow around a circular cylinder where the eddies are located behind the cylinder, the flow conditions in the fusion zone lead to the formation of eddies at the weld pool boundary. This phenomenon causes a narrow jet of liquid material at high velocities on the centre line behind the keyhole which leads to elongated weld pools and isotherms. In this flow regime, the convective heat transfer in the molten material plays a
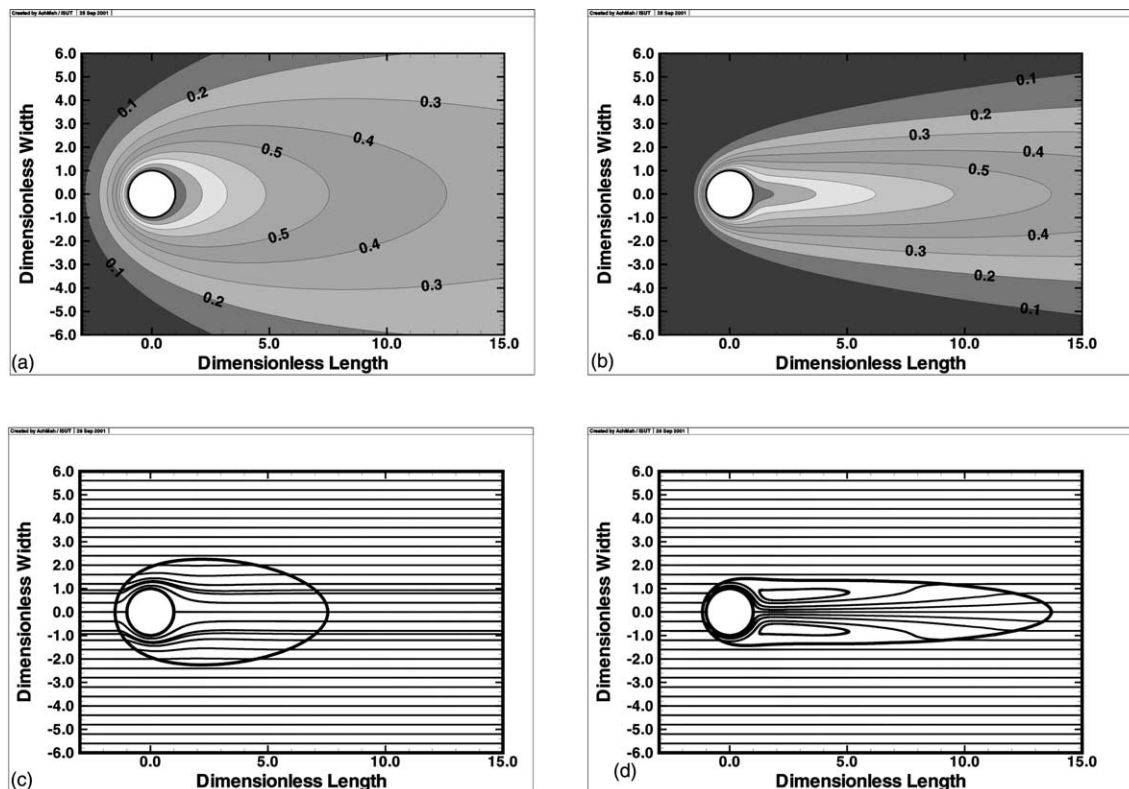
Fig. 5. Computed temperature and velocity fields for $Pr = 0.1$, $\Theta_m = 0.5$ and different Péclet numbers: $Pe = 1.0$ (a,c) and $Pe = 4.0$ (b,d).
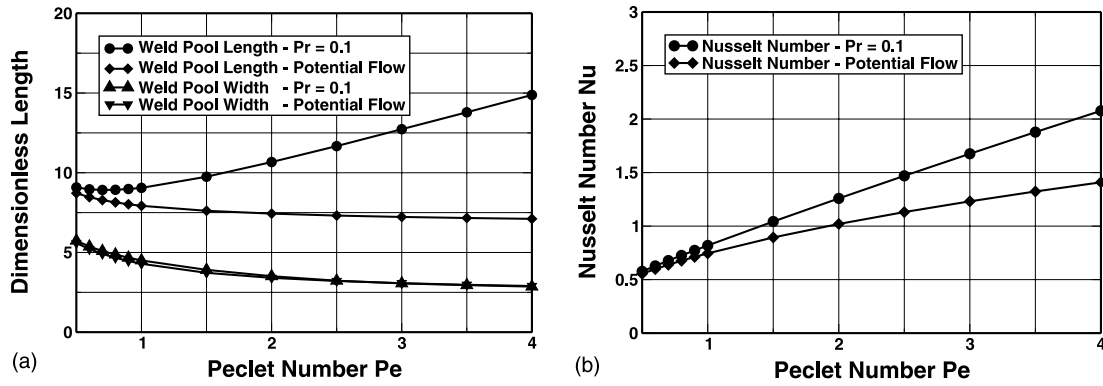
Fig. 6. Calculated weld pool dimensions (a) and calculated Nusselt numbers (b) in dependence on the Péclet number for $Pr = 0.1$ and $\Theta_{melt} = 0.5$.

dominant role for the prediction of the weld pool length as well as the absorbed laser power transported across the keyhole boundary. The latter can be characterized by the average Nusselt number Nu_m which is defined as

$$Nu_m = -\frac{1}{2\pi Z_{max}} \int_0^{Z_{max}} \int_0^{2\pi} \frac{\partial \Theta}{\partial R}\bigg|_{key} d\varphi \, dZ. \qquad (16)$$

In Fig. 6, calculated weld pool dimensions and calculated Nusselt numbers in dependence on the Péclet number are shown. The importance of an accurate description of the fluid motion, driven by the flow around the keyhole, shows the comparison with a simplified

computation of the temperature field using the analytical solution of the potential flow around a cylinder as approximation for the velocity distribution. For Péclet numbers $Pe > 1$, the differences between the calculated values are significant. Only the calculated weld pool width shows a good agreement.

For a material with a known Prandtl number it is to be expected that the eddies at the melt pool boundary behind the keyhole become unstable at a definite Péclet number. This phenomenon limits the welding travel speed and can explain instabilities in the melt pool flow which influence the quality of the welding seam
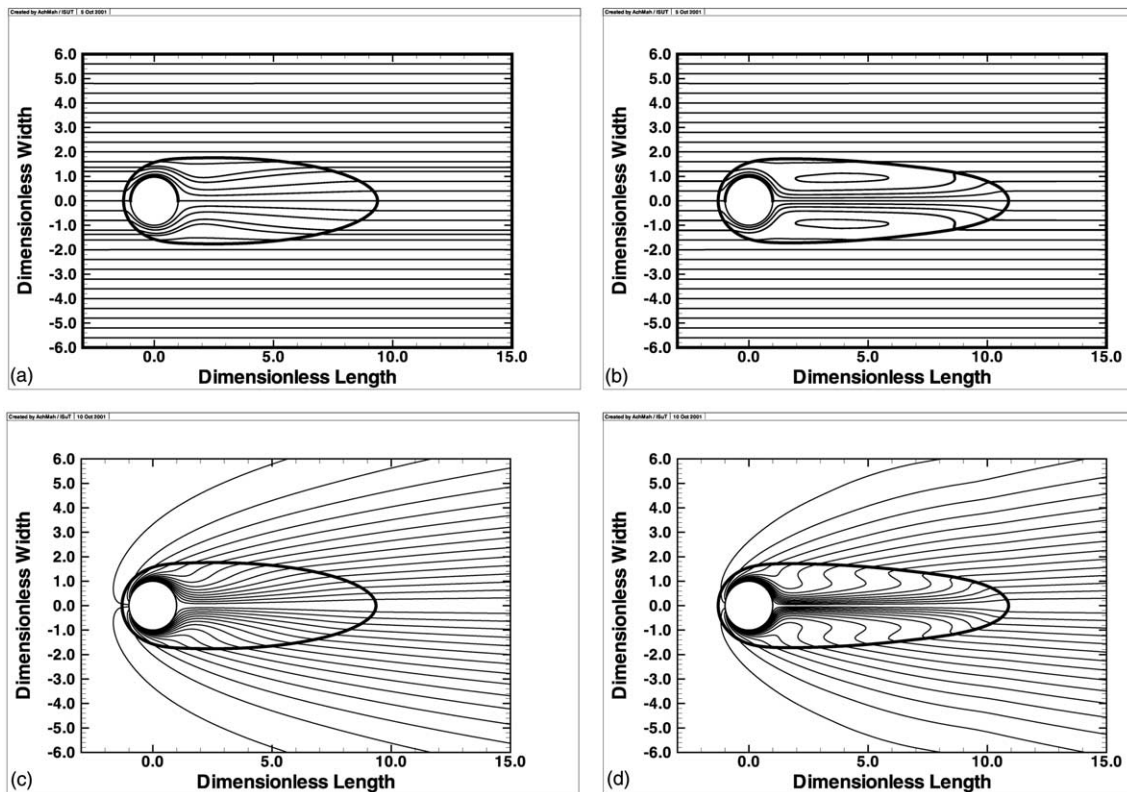
Fig. 7. Computed velocity fields (a,b) and distributions of the heat function (c,d) for $Pe = 2.0$, $\Theta_m = 0.5$ and different Prandtl numbers: $Pr = 0.1$ (a,c) and $Pr = 0.025$ (b,d).

unfavourably. The maximum Péclet number is strongly influenced by the value of the Prandtl number which determines the Reynolds number in the fusion zone. Fig. 7a and b show the velocity distribution for a variation of this parameter. It can be seen that small values of the Prandtl number and high numbers of the Reynolds number respectively favour the formation of eddies. Additionally, an illustration of the heat function for the same parameters is shown. The heat function describes the direction of energy tranfer (Griebel et al., 1995). It shows the influence of the convective heat transfer on the local energy transport very clearly.

In the characteristic parameter range for welding of steels, the two-dimensional simulation does not allow a sufficient prediction of the weld pool dimensions in agreement with experimental measurements. Especially, the calculated weld pool widths are too small. The differences are to be attributed to the influence of buoyancy and friction forces as well as surface tensions. Computed temperature and velocity distributions with consideration of these effects are shown in Fig. 8 for $Pe = 1$, $Pr = 0.1$ and $\Theta_m = 0.5$. For the illustration of the velocity fields a uniform vector length is used. Fig. 8a shows the influence of buoyancy forces for a Grashof number $Gr = 1000$. The melt ascends on the hotter keyhole boundary and a eddie is formed behind the keyhole. This leads to an expansion of the fusion zone in the top surface area. However, typical Grashof numbers in the melt pool area of steels are in the range of $Gr < 100$, and it is mostly possible to neglect buyoyancy forces.

More important for laser beam welding of steels is the influence of surface tension gradients. Fig. 8b and c show computed temperature and velocity fields for a Marangoni number $Ma = 1000$ without and with consideration of surface active elements. In the first case, for a constant and negative value of the temperature coefficient of surface tension, the melt flows from the hotter keyhole boundary to the colder melt pool boundary and this leads to an expansion of the fusion zone in the area of the top and the bottom surface. In the second case, the sign change of the coefficient of surface tension leads to a reversal of the flow at a certain temperature which depends on the given concentration of the surface active element. This behaviour can cause bulbous weld pool shapes with a maximum extension in the middle of the transverse section of the weld seam. It is to be expected that surface tension gradients have the most controlling effect on the weld pool shape and size and the accurate modelling plays an important role for different fusion welding methods (Lei et al., 1998; Pitscheneder et al., 1998; Fuhrich et al., 1999; Mahrle et al., 2000).

In the case of deep penetration laser beam welding, friction forces have to be taken into consideration too. It
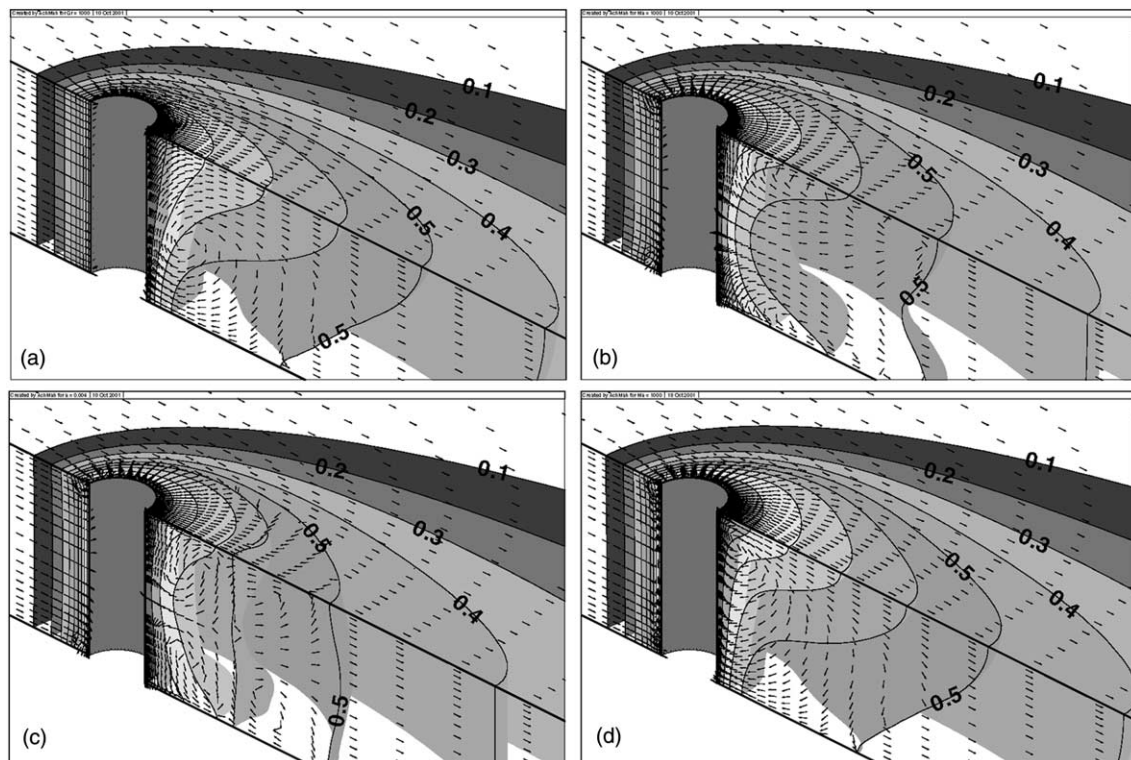
Fig. 8. Temperature and velocity distribution in dependence on different weld pool phenomena for $Pe = 1.0$, $Pr = 0.1$, $\Theta_m = 0.5$ and $Z_{max} = 5$. Buoyancy forces: $Gr = 1000$ and $Ma = W_{key} = 0$ (a). Surface tensions: $Ma = 1000$ with $a = 0.000$ and $Gr = W_{key} = 0$ (b), $Ma = 1000$ with $a = 0.004$ and $Gr = W_{key} = 0$ (c). Friction forces: $W_{key} = 10$ and $Gr = Ma = 0$ (d).
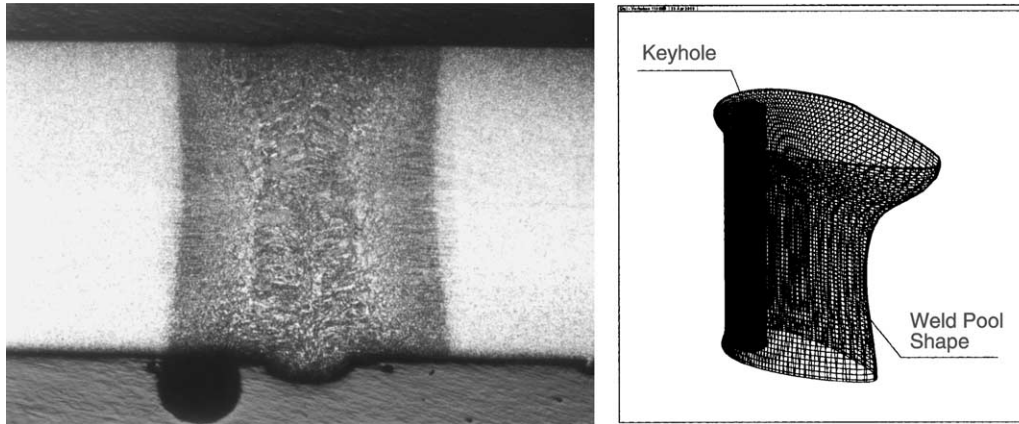
Fig. 9. Transverse macrosection of a laser beam welded joint for a low-alloyed steel and computed weld pool shape for the given welding parameters. Steel St-52, $h = 5$ mm, $P_L = 5000$ W, $w_{ch} = 0.0133$ m/s.

induces a vertical acceleration of the melt at the keyhole boundary due to the interactions between metal vapour flow escaping from the keyhole and melt pool flow (Beck, 1996). Fig. 8d shows the calculated temperature and velocity field for $W_{key} = 10$. Proper values for this velocity are to be determined in combination with experiments.

It can be summerized that the prediction of the local temperature distribution in the heat-affected zone of laser beam welded joints usually requires a three-dimensional simulation. Mention should be made on the fact that for the determination of the dimensionless groups the knowledge of all relevant properties is necessary. In this context, on the one hand the assumption of constant averaged values in the molten zone is a necessity because exact data as a function of the temperature are missed and on the other this approximation enables the correlation with experiments by the choice of suitable values.

4. Verification and validation

For the verification of the developed simulation program various test cases were examined in comparison with analytical solutions and experimental investigations (Mahrle, 2000). In the case of the computation of the coupled temperature and velocity fields under conditions relevant to the described welding process, it was especially necessary to use a highly enough resolved grid, so that any numerical uncertainties can be excluded. As a result of these investigations, the grid independence of the numerical solution is ensured.

By means of the validation it is additionally to verify whether the model in combination with the used material functions is able to reflect experimental results in a desired accuracy. For that purpose welding experiments with different steel sheets has been executed and the

numerically and experimentally seam shapes as well as the seam widths on the top and the bottom side were compared. Exemplarily, Fig. 9 shows the transverse macrosection of a laser beam welded joint for a low-alloyed steel and the computed weld pool shape with consideration of all discussed effects including phase change and temperature dependent properties in the solid state. The used reference values for the material properties of the molten zone are given in Table 1. The variation of the density ϱ^*, the specific heat capacity c^* and the heat conductivity λ^* between environmental and melting point temperature as well as the variation of the melting point temperature as function of the steel composition are considered for the different types of steel (Richter, 1973).

The simulation model describes obviously the local heat transfer in the fusion zone and thus the weld pool shape qualitatively very well. The extension of the seam width on the top and bottom surface can be explained by the effect of surface tensions and the fact of the greater width on the top side can be put down to the influence of friction forces as a result of the metal vapour flow escaping from the capillary.

The comparison between measured and calculated values of the seam width as function of the welding travel speed shows also a good agreement for different types of steel (see Fig. 10). The variation of the experimentally determined values at the same welding velocity can be explained by the possible unsteady behaviour of the keyhole and the weld pool flow. The marked zone,

Table 1
Material properties of liquid iron at reference temperature

Heat conductivity, λ_0	35.0 $\mathrm{W m^{-1} K^{-1}}$
Specific heat capacity, c_0	800.0 $\mathrm{J kg^{-1} K^{-1}}$
Density, ϱ_0	7200 $\mathrm{kg m^{-3}}$
Thermal diffusivity, a_0	$6.0 \times 10^{-6} \mathrm{m^2 s^{-1}}$
Kinematic viscosity, v	$6.0 \times 10^{-7} \mathrm{m^2 s^{-1}}$
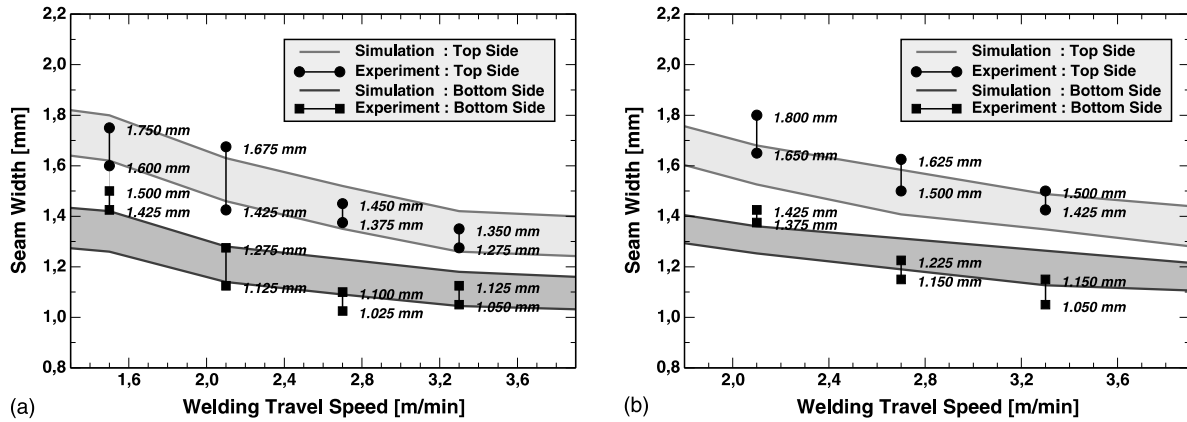
Fig. 10. Comparison between experimentally measured and calculated seam widths in dependence on the welding travel speed for a low-alloyed steel St-52 (a) and a stainless steel X5CrNi1810. (b) $h = 3$ mm, $P_L = 5000$ W.

predicted by the simulation in dependence on the welding travel speed, results from two different keyhole radii which were used as the decisive model parameter for the necessary calculations of the characteristic dimensionless groups for the given material and the given technological parameters of the welding process.

5. Summary and outlook

The presented three-dimensional model of the laser beam welding process enables in combination with the implemented solution method the computation of the local temperature field in agreement with experimental results. Using the developed simulation program, questions regarding the influence of different transport phenomena in the fusion zone on the weld pool shape and size can be answered. Additionally, the analysis of the simulated temperature distribution allows the calculation of the energy transported across the keyhole boundary. Using the characteristic Nusselt number (see Eq. (16)), the theoretical absorbed power $P_{L,abs}$ for a given set of parameters can be calculated according to the following equation:

$$P_{L,abs} = 2\pi h \lambda_0 (\vartheta_v - \vartheta_u) Nu_m, \qquad (17)$$

where h is the plate thickness. Of course, with regard to the model assumptions, the presented simulation tool does not allow statements about the laser power or other processing parameters which are necessary for the keyhole formation or its stability during the welding process. However, the analyzing of the computed temperature distribution enables estimations of the welding efficiency $\eta_L = P_{L,abs}/P_L$ under proper processing conditions according to Eq. (17).

The applicability and accuracy of the developed simulation model was investigated for different types of steel. In principle, the application to other weldable materials is possible under the precondition of the

availability of the necessary material properties. Furthermore, the assumption of an approximately constant keyhole radius for through-welding processes must be fulfilled.

Up to now the computation of the temperature distribution is concentrated to the fusion zone. Future work will be focussed on a coupling of the presented process model with a simulation routine which calculate the transient temperature field in a given welding construction as precondition for the determination of cooling rates and cooling times, respectively. The knowledge of these quantities is necessary for the simulation of microstructural states, residual stresses and distortions. An algorithm for the simultaneous computation has been proposed on the basis of the Chimera overset grid technique (Weiss et al., 2000).

References

Beck, M., 1996. Modellierung des Lasertiefschweißens, Dissertation, Universität Stuttgart. Teubner Verlag, Stuttgart.

Beck, M., Berger, P., Hügel, H., 1992. Modelling of keyhole melt interaction in laser deep penetration welding. In: Mordike, B.L. (Ed.), European Conference on Laser Treatment of Materials. DGM Informationsgesellschaft, Oberursel.

Becker, D., 1995. Wechselwirkung von Wärmeleitung, Schmelzbaddynamik und Verdampfung beim Tiefschweißen mit Laserstrahlung, Dissertation, RWTH Aachen, Aachen, Shaker.

Berger, P., 1993. Physical models on deep penetration laser beam welding with emphasis on fluid dynamics. In: Fotakis, C., Kalpouzos, C., Papazoglou, T. (Eds.), 9th International Symposium on Gas Flow and Chemical Lasers 1992, SPIE vol. 1810.

Dowden, J., Davis, M., Kapadia, P.D., 1995. The flow of heat and the motion of the weld pool in penetration welding with a laser. J. Appl. Phys. 57 (9).

Dowden, J., Kapadia, P.D., Davis, M., 1987. The fluid dynamics of laser welding. In: Cheremisinoff, N.P. (Ed.), Encyclopedia of Fluid Dynamics. Gulf Publication Company, Houston.

Fuhrich, T., Kern, M., Berger, P., Hügel, H., 1999. Influence of the surface tension gradient on the shape of the weld pool in laser beam welding. In: Kaplan, A., Schuöker, D. (Eds.), Proceedings on

Mathematical Modelling of Material Processing with Lasers. TU Wien/ISLT, Wien.

Griebel, M., Dornseifer, T., Neunhoeffer, T., 1995. Numerische Simulation in der Strömungsmechanik. Vieweg, Braunschweig, Wiesbaden.

Hügel, H., 1992. Strahlwerkzeug Laser. B.G. Teubner, Stuttgart.

Hügel, H., Dausinger, F., Berger, P., Beck, M., Griebsch, J., 1994. Investigations on fundamental phenomena as basis for high quality laser welding. In: Proceedings of the 5th European Conference on Laser Treatment of Materials, DVS-Berichte, Bd. 163. DVS-Verlag, Düsseldorf.

Kern, M., Fuhrich, T., Berger, P., Hügel, H., 1998. Dreidimensionale Simulation der Kapillarausbildung und der Schmelzbadströmung beim Laserstrahlschweißen. In: Sepold, G., Geiger, M. (Eds.), Strahl-Stoff-Wechselwirkung bei der Lasermaterialbearbeitung, Bd. 6. Bremen, Bias Verlag.

Kroos, J., 1993. Stabilität und Dynamik der Dampfkapillare beim Laserstrahlschweißen von Metallen. Dissertation, Technische Universität Braunschweig.

Kroos, J., Gratzke, U., Simon, G., Vicanek, M., 1992. Dynamic behaviour of the keyhole in laser welding. J. Phys. D: Appl. Phys. 26.

Lei, Y.P., Shi, Y.W., Murakawa, H., Ueda, Y., 1998. Numerical analysis on the effect of sulphur content on weld pool geometry and free surface phenomena for type 304 stainless steel. In: Cerjak, H., Badeshia, H.K.D.H. (Eds.), Mathematical Modelling of Weld Phenomena 4. IOM Communications Ltd., London.

Mahrle, A., Schmidt, J., 1998a. Numerical Simulation of the Temperature Distribution During Deep Penetration Laser Beam Welding Using Dimensionless Groups. In: Cerjak, H., Badeshia, H.K.D.H. (Eds.), Mathematical Modelling of Weld Phenomena 4. IOM Communications Ltd., London.

Mahrle, A., Schmidt, J., 1998b. Numerical simulation of weld pool convection during deep penetration laser beam welding. In: Papailiou, K.D., Tsahalis, D., Périaux, J., Hirsch, C., Pandolfi, M. (Eds.), Computational Fluid Dynamics 98. John Wiley & Sons Ltd., Chichester.

Mahrle, A., 2000. Einfluß des konvektiven Energietransportes auf die lokale Temperaturverteilung beim Laserstrahlschweißen, Dissertation, Universität Magdeburg. Shaker, Aachen.

Mahrle, A., Schmidt, J., 2000. Three-dimensional weld pool simulation in laser beam welding. In: Rahman, M., Brebbia, C.A. (Eds.), Advances in Fluid Dynamics III. WIT Press, Southampton, Boston.

Mahrle, A., Schmidt, J., 2001. Heat and mass transfer in the fusion zone of laser beam welding processes. In: de Vahl Davis, G., Leonardi, E. (Eds.), CHT'01—Advances in Computational Heat Transfer II, vol. 2. Begell House Inc., New York, Wallingford, pp. 697–704.

Mahrle, A., Schmidt, J., Weiss, D., 2000. Influence of marangoni convection on weld pool shape and temperature distribution in laser beam welding. In: Hahne, E.W.P., Heidemann, W., Spindler, K. (Eds.), 3rd European Thermal Sciences Conference 2000. Edizioni ETS, Pisa.

Matsunawa, A., Kim, J.D., Selo, N., Mizutani, M., Katayarna, S., 1998. Dynamics of Keyhole and Molten Pool in Laser Welding. J. Laser Appl. 10 (6).

Naue, G., Bärwolff, G., 1992. Transportprozesse in Fluiden. Deutscher Verlag für Grundstoffindustrie, Leipzig.

Pitscheneder, W., Ebner, R., Hong, T., DebRoy, T., Mundra, K., Benes, R., 1998. Experimental and numerical investigation of transport phenomena in conduction mode weld pools. In: Cerjak, H., Badeshia, H.K.D.H. (Eds.), Mathematical Modelling of Weld Phenomena 4. IOM Communications Ltd., London.

Radaj, D., 1992. Heat Effects of Welding—Temperature Field, Residual Stress, Distortion. Springer, Berlin.

Radaj, D., 1999. Schweißprozeßsimulation—Grundlagen und Anwendungen. Verlag für Schweißen und Verwandte Verfahren, Düsseldorf.

Richter, F., 1973. Die wichtigsten Eigenschaften von 52 Eisenwerkstoffen. Düsseldorf, Stahleisen.

Sahoo, P., DebRoy, T., McNallan, M.J., 1988. Surface tension of binary metal-surface active solute systems under conditions relevant to welding metallurgy. Metall. Trans. B 19B, 483–491.

Sudnik, W., Radaj, D., Erofeew, W., 1996. Computerized Simulation of Laser Beam Welding—Modelling and Verification. J. Phys. D: Appl. Phys. 29, 2811–2817.

Sudnik, W., Radaj, D., Erofeew, W., 1998. Computerized simulation of laser beam weld formation comprising joint gaps. J. Phys. D: Appl. Phys. 31, 3475–3480.

Weiss, D., Mahrle, A., Schmidt, J., 2000. Simulation of welding processes based on micro models. In: Sundén, B., Brebbia, C.A. (Eds.), Heat Transfer VI. WIT Press, Southampton, Boston.

Winkler, C., Amberg, G., Inoue, H., Koseki, T., 1998. A numerical and experimental investigation of qualitatively different weld pool shapes. In: Cerjak, H., Badeshia, H.K.D.H. (Eds.), Mathematical Modelling of Weld Phenomena 4. IOM Communications Ltd., London.